

A local polynomial moment approximation for compartmentalised biochemical systems

Tommaso Bianucci^{1,2} and Christoph Zechner^{1,2,3,*}

¹Max Planck Institute of Molecular Cell Biology and Genetics, Pfotenhauerstraße 108, 01307 Dresden, Germany

²Center for Systems Biology Dresden, Pfotenhauerstraße 108, 01307 Dresden, Germany

³Cluster of Excellence Physics of Life, TU Dresden, Arnoldstraße 18, 01307 Dresden, Germany

*Correspondence to: zechner@mpi-cbg.de

June 15, 2023

Abstract: Compartmentalised biochemical reactions are a ubiquitous building block of biological systems. The interplay between chemical and compartmental dynamics can drive rich and complex dynamical behaviors that are difficult to analyse mathematically – especially in the presence of stochasticity. We have recently proposed an effective moment equation approach to study the statistical properties of compartmentalised biochemical systems. So far, however, this approach is limited to polynomial rate laws and moreover, it relies on suitable moment closure approximations, which can be difficult to find in practice. In this work we propose a systematic method to derive closed moment dynamics for compartmentalised biochemical systems. We show that for the considered class of systems, the moment equations involve expectations over functions that factorize into two parts, one depending on the molecular content of the compartments and one depending on the compartment number distribution. Our method exploits this structure and approximates each function with suitable polynomial expansions, leading to a closed system of moment equations. We demonstrate the method using three systems inspired by cell populations and organelle networks and study its accuracy across different dynamical regimes.

1 Introduction

Compartmentalisation of biochemical reactions is one of the most characteristic and fundamental properties of living systems. It occurs hierarchically across length scales, ranging from organs and tissues, down to cells and subcellular structures. Compartmentalisation provides functional segregation in space and time and allows for modularity in the assembly of larger scale structure and function.

Compartmentalised reaction systems can be described as populations of enclosed volumes (e.g., organelles or cells) that evolve with time. Individual compartments contain molecules that can undergo chemical reactions, while the compartments themselves can exhibit temporal dynamics as well. As an ex-

ample, two compartments may fuse or divide, or new compartments may be created or exit the system as observed in organelle networks for instance [1]. The combination of chemical reactions and compartment dynamics results in challenging multiscale problems, which attracted substantial interest in the past.

Population balance equations (PBEs) provide a general mathematical framework to describe a broad class of compartmentalized reaction systems [2, 3]. In the context of biology, they have been applied to endosomal networks [4], heterogeneous cell populations [5, 6] and clone-size dynamics [7] to name a few. PBEs are typically formulated in the thermodynamic limit and as such apply to systems where fluctuations at both the chemical and compartmental level are negligible. While stochastic systems have also been considered within the population balance framework [8, 3], they are typically accessible only through computationally expensive Monte Carlo simulation.

In recent years, there has been increased interest in the theoretical and computational analysis of compartmentalized reaction systems in the presence of stochasticity [9, 10, 11, 12, 13, 14]. In contrast to bulk chemical systems, stochasticity arises at two levels in these systems. First, chemical reactions inside individual compartments take place at random times, leading to random variations in each compartment's state [15]. Second, compartment events such as intake, division or turnover exhibit stochasticity such that the population size fluctuates with time. Most existing computational approaches to analyze compartmentalized reaction systems focus on models of cell populations, where intracellular processes are combined with population-level dynamics such as cell growth, division or phenotypic selection [16, 9, 17, 11, 18]. Since the number of cells is typically large in these systems, one can consider the limit of infinitely large populations, where fluctuations in the population-level dynamics become negligible. An important consequence of this limit is that the entire population can be described by a single probability density function $p(x, t)$, which

captures how the compartment state is distributed across the population at time t . The dynamics of $p(x, t)$ can then be derived and solved using direct numerical integration [19, 20] or moment approximation techniques [11].

The situation becomes more complex when the number of compartments is small, such that the limit of large populations is no longer applicable. This can be the case for organelle networks inside cells, or small cell communities at early developmental stages. When the population size is finite, the distribution of compartment states for a particular population is a stochastic object, which at a given time t depends on the state of all compartments present in the population. Calculating the probability distribution over the full population state would be exceedingly challenging due to the combinatorial explosion of states in such systems. Moreover, such high-dimensional object would be difficult to work with and analyze in practice. To address these challenges, we have recently proposed a more effective approach, which summarizes the high-dimensional population state in terms of a small number of population moments, such as the total number of compartments, or the total amount of a certain molecule across the population [10]. A key difference to the moment techniques mentioned above is that the resulting moments are stochastic, which is a consequence of the finite population size. To effectively access the statistical properties of the compartment population, we derived ordinary differential equations which capture the mean and variance of the stochastic population moments. As with conventional moment-based techniques, the resulting system of equations is not necessarily closed, which we have so far addressed using *ad hoc* moment-closure approximations [10].

There are two main limitations of this approach. First, identifying suitable closure functions can be difficult in practice as they are typically found in a trial-and-error fashion. Second, it is currently restricted to systems with polynomial rate laws to ensure that the resulting moment equation hierarchy is self-contained [21, 10]. In the present work, we develop a systematic moment-approximation technique which aims at addressing these two issues. The approach is based on a local polynomial approximation of the underlying rate-laws, which for the considered class of systems factorizes into a product of two functions that depend on the compartment content and compartment number distribution, respectively. The resulting scheme always leads to a closed set of moment equations and is applicable also to systems involving non-polynomial rate-laws. We demonstrate our approach using several biologically-inspired models and analyze its accuracy and runtime. Our implementation of the moment-approximation technique is publicly available through a new release of our previously developed symbolic moment generator *Compactor* [22].

2 Results

2.1 Stochastic compartment populations

To describe the dynamics of a stochastic compartment population, we make use of our previously proposed formalism [10]. We define a compartment population as a collection of N distinct entities, each one being associated with a d -dimensional content variable $x \in \mathbb{X} \subseteq \mathbb{N}^d$. Individual dimensions of x typically correspond to the copy number of a particular chemical species, but could encode also other discrete-valued features, such as compartment categories (e.g., cell types).

The state of the population can be represented by a *number distribution* function $n : \mathbb{X} \rightarrow \mathbb{N}$ that maps any possible value of the content variable x to the number of compartments $n(x)$ having that particular content. The number distribution can be represented by a (typically infinite) multidimensional array $\mathbf{n} = (n(x))_{x \in \mathbb{X}}$, where the compartment number $n(x)$ corresponds to the element of \mathbf{n} at index x , i.e. $\mathbf{n}_x = n(x)$.

The compartment population can change dynamically according to a set of *transition classes*. Transition classes can encode changes in both the molecular content of a compartment and in the population of compartments itself: for instance two molecules may react to produce a third one within one compartment, or two compartments may fuse into a single one, merging their contents. Transition classes therefore generalise the concept of *reactions* to compartmentalised systems.

A transition class c is defined by a set $x_c = \{x_c^{(1)}, \dots, x_c^{(r_c)}\}$ of reactant compartments, a set $y_c = \{y_c^{(1)}, \dots, y_c^{(p_c)}\}$ of product compartments and by a rate function $h_c(\mathbf{n}(t), x_c, y_c)$ which determines how likely a transition with a particular combination of reactant and product compartments occurs per unit time. Throughout this work, we consider the compartment population to exhibit Markovian dynamics such that the rate functions depend only on the current state of the population $\mathbf{n}(t)$.

Consider a compartment population whose dynamics follows a set of transition classes \mathcal{C} . The time evolution of the number distribution can then be described as

$$\mathbf{n}(t) = \mathbf{n}(0) + \sum_{c \in \mathcal{C}} \sum_{x_c, y_c} \Delta \mathbf{n}_c(x_c, y_c) R_{c, x_c, y_c}(t) \quad (1)$$

where $\mathbf{n}(0)$ is the initial state of the population at $t = 0$ and $R_{c, x_c, y_c}(t)$ are counting processes with rate function $h_c(\mathbf{n}(t), x_c, y_c)$ tracking the number of transitions of type c involving the particular sets of reactant- and product compartment x_c and y_c up to time t . The array $\Delta \mathbf{n}_c(x_c, y_c) = (-\sum_{x \in x_c} \delta_{x, s} + \sum_{y \in y_c} \delta_{y, s})_{s \in \mathbb{X}}$ captures how the population state $\mathbf{n}(t)$ changes when this particular transition happens. The process defined in (1) can be understood as an instance of a measure-valued stochastic process [23, 24]. Note that for compactness, we will drop the time-dependency of $\mathbf{n}(t)$ and all derived quantities in the following.

Throughout this work, we consider rate functions of the form

$$h_c(\mathbf{n}, x_c, y_c) = k_c \pi_c(y_c | x_c) g_c(x_c) w_{c, x_c}(\mathbf{n}), \quad (2)$$

with k_c as a rate constant, g_c as a function that depends exclusively on the content of the reactant compartments and $w_{c,x_c} := w_c(n(x_c^{(1)}), \dots, n(x_c^{(r_c)}))$ as a function that depends only on the population state \mathbf{n} . Throughout this work, we consider w_{c,x_c} to be a multilinear polynomial, which arises combinatorially by counting all indistinguishable combinations of reactant compartments for a particular population state \mathbf{n} . We refer to functions w_{c,x_c} defined in this way as *mass-action-like*. The function π_c denotes the *outcome distribution* that determines how likely a particular set of product compartments is realized from a given set of reactant compartments. In the case of cell division, for examples, π_c describes the partitioning of molecular content between daughter cells given the content of the mother cell right before division. Concrete examples of transition classes and their rate functions will be provided later in our case studies.

We can observe from eq. (2) that the transition rate functions in the considered systems are *separable*: they factorise into a product of a function that depends on the content of the involved compartments and another function that depends on how many such compartments are available in the population. We can therefore write

$$h_c(\mathbf{n}, x_c, y_c) = f_c(x_c, y_c) w_{c,x_c}(\mathbf{n}) \quad (3)$$

where $f_c(x_c, y_c)$ only depends on the content of the reactant and product compartments and $w_{c,x_c}(\mathbf{n})$ depends explicitly only on the number of compartments with the given contents (x_c), but not on the content itself.

2.2 Moment dynamics

While eq. (1) describes the time evolution of the full population state, this equation is difficult to deal with in practice. A more effective way to analyze compartmentalized systems is provided by moment equations, which capture certain statistical properties of the compartment population [3, 10, 11]. We define a *population moment* of exponent $\gamma \in \mathbb{N}^d$ by

$$M^\gamma = \sum_x x^\gamma \mathbf{n}_x = \sum_x x_1^{\gamma_1} x_2^{\gamma_2} \dots x_d^{\gamma_d} \mathbf{n}_x. \quad (4)$$

The *order* of this moment is given by $|\gamma|$, which is the sum of all elements of the multi-index γ . Note that a population moment is a functional of the stochastic number distribution \mathbf{n} and correspondingly, is itself stochastic [10].

A special population moment is the moment of order zero M^0 , which counts the total number of compartments present in the system. In the following, we will refer to this moment as $N := M^0$. Similarly, a moment of order one, i.e., M^{e_j} with e_j as the j -th unit vector, counts the total amount of the j -th species across all compartments.

Starting from eq. (1), we can now derive a stochastic differential equation which captures the time-evolution of a population moment M^γ ,

$$dM^\gamma = \sum_{c \in \mathcal{C}} \sum_{x_c, y_c} \Delta M_c^\gamma(x_c, y_c) dR_{c,x_c, y_c}, \quad (5)$$

where $\Delta M_c^\gamma(x_c, y_c) = \sum_s s^\gamma \Delta n_{c,x_c, y_c}(s)$ denotes the instantaneous change of the moment M^γ when the transition with compartment sets x_c and y_c from class c happens. In practice, it is useful to study the expected behavior of a stochastic population moment. To this end, we can take the expectation on both sides of eq. (5), which yields

$$\frac{d\langle M^\gamma \rangle}{dt} = \sum_c \left\langle \sum_{x_c, y_c} \Delta M_c^\gamma(x_c, y_c) h_c(\mathbf{n}, x_c, y_c) \right\rangle. \quad (6)$$

Eq. (6) is an ordinary differential equation that describes the time-evolution of the *expected moment* $\langle M^\gamma \rangle$ and we refer to it as *moment equation* throughout this work.

Using the separability of h_c we can rewrite eq. (6) as

$$\frac{d\langle M^\gamma \rangle}{dt} = \sum_c \left\langle \sum_{x_c, y_c} \Delta M_c^\gamma(x_c, y_c) f_c(x_c, y_c) w_{c,x_c}(\mathbf{n}) \right\rangle. \quad (7)$$

Recalling eq. (2), we can further split the function $f_c(x_c, y_c)$ into a product $\pi_c(y_c | x_c) g_c(x_c)$, where the rate function $g_c(x_c)$ only depends on the content of the reactant compartments, which is then multiplied by the probability π_c of obtaining specific product compartments y_c . If we now carry out the summation over y_c , we obtain an expectation over ΔM_c^γ conditionally on x_c . In particular, we obtain

$$\begin{aligned} \frac{d\langle M^\gamma \rangle}{dt} &= \sum_c \left\langle \underbrace{\sum_{x_c} \sum_{y_c} \Delta M_c^\gamma(x_c, y_c) \pi_c(y_c | x_c)}_{\mathbb{E}_{\pi_c}[\Delta M_c^\gamma(x_c, y_c) | x_c]} g_c(x_c) w_{c,x_c}(\mathbf{n}) \right\rangle \\ &= \sum_c \left\langle \sum_{x_c} \underbrace{\mathbb{E}_{\pi_c}[\Delta M_c^\gamma(x_c, y_c) | x_c]}_{\Delta M_c^\gamma(x_c)} g_c(x_c) w_{c,x_c}(\mathbf{n}) \right\rangle \\ &= \sum_c \left\langle \sum_{x_c} \Delta M_c^\gamma(x_c) g_c(x_c) w_{c,x_c}(\mathbf{n}) \right\rangle \\ &= \sum_c \left\langle \sum_{x_c} f_c^\gamma(x_c) w_{c,x_c}(\mathbf{n}) \right\rangle, \end{aligned} \quad (8)$$

$$= \sum_c \left\langle \sum_{x_c} f_c^\gamma(x_c) w_{c,x_c}(\mathbf{n}) \right\rangle, \quad (9)$$

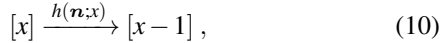
showing that the individual summands are again separable into two functions that depend only on the compartment content and the number distribution, respectively. In the following, we refer to f_c^γ and w_{c,x_c} as *content-* and *state function*, respectively. Moment equations for generic products of moments (e.g., N^2) exhibit the same separability, such that the following results that are based on the separability property can be applied to them as well (A).

2.3 Challenges of deriving moment equations in practice

When deriving moment equations for a particular system, we can use eq. (9). The two functions, f_c^γ and w_{c,x_c} , can be directly

derived from the specifications of a given transition class c and for any given moment exponent γ . However, difficulties may arise depending on their particular form. These difficulties can be best explained by going through a series of representative examples.

Linear content- and state function. The simplest scenario occurs when both the content- and state functions are at most linear polynomials. In this case the resulting moment dynamics is always closed, similarly to what happens in moment equations for bulk chemical systems. As an example, let us consider a simple degradation reaction occurring within the compartments



with $h(\mathbf{n};x) = x \mathbf{n}_x$ and assume that we are interested in analyzing the moments N and M^1 . The state function is given by

$$w_{c,x_c} = \mathbf{n}_x \quad (11)$$

and the content functions associated with N and M^1 are

$$f_c^0(x) = \Delta M_c^0 g_c(x) = 0 \cdot x \quad (12)$$

$$\text{and } f_c^1(x) = \Delta M_c^1 g_c(x) = -1 \cdot x, \quad (13)$$

respectively. The moment equations for $\langle N \rangle$ and $\langle M^1 \rangle$ are therefore given by

$$\frac{d\langle N \rangle}{dt} = \left\langle \sum_x 0 \cdot x \cdot \mathbf{n}_x \right\rangle = 0 \quad (14)$$

$$\frac{d\langle M^1 \rangle}{dt} = \left\langle \sum_x -1 \cdot x \cdot \mathbf{n}_x \right\rangle = -\langle M^1 \rangle, \quad (15)$$

which can be readily solved. This is because for linear content- and state functions, the moments appearing on the right-hand side of the equations cannot be of higher order than those on the left-hand side, ensuring that the resulting moment dynamics is closed.

Nonlinear content function. We next consider a more complex scenario, where the state function is still linear, while the content function is a polynomial of higher degree. As an example, we consider the case where compartments exit the system with a rate that again linearly depends on their content:



with $h(\mathbf{n};x) = x \mathbf{n}_x$. The relevant content- and state functions are now given by

$$f_c^0(x) = \Delta M_c^0 g_c(x) = -1 \cdot x = -x \quad (17)$$

$$f_c^1(x) = \Delta M_c^1 g_c(x) = -x \cdot x = -x^2 \quad (18)$$

$$w_{c,x_c}(\mathbf{n}) = \mathbf{n}_x \quad (19)$$

and the equations for $\langle N \rangle$ and $\langle M^1 \rangle$ become

$$\frac{d\langle N \rangle}{dt} = \left\langle \sum_x -x \cdot \mathbf{n}_x \right\rangle = -\langle M^1 \rangle \quad (20)$$

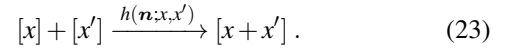
$$\frac{d\langle M^1 \rangle}{dt} = \left\langle \sum_x -x^2 \cdot \mathbf{n}_x \right\rangle = -\langle M^2 \rangle. \quad (21)$$

In this case, the equation for $\langle M^1 \rangle$ depends on the additional moment $\langle M^2 \rangle$ because the content function $f_c^1(x)$ is a second degree polynomial. Deriving the equation for $\langle M^2 \rangle$ yields

$$\frac{d\langle M^2 \rangle}{dt} = \left\langle \sum_x -x^2 \cdot x \cdot \mathbf{n}_x \right\rangle = -\langle M^3 \rangle, \quad (22)$$

which in turn depends on the additional moment $\langle M^3 \rangle$. More generally, it turns out that the equation for any $\langle M^k \rangle$ depends on $\langle M^{k+1} \rangle$, leading to an infinite-dimensional system of moment equations. This phenomenon is generally known as *closure problem* [21, 3].

Nonlinear state function. We now consider a scenario where the state function is nonlinear. This is for instance the case when two compartments fuse, i.e.,



In this case, the state function is

$$w_{(x,x')}(\mathbf{n}) = \frac{\mathbf{n}_x(\mathbf{n}_{x'} - \delta_{x,x'})}{(1 + \delta_{x,x'})}, \quad (24)$$

which counts the number of all possible interactions of two reactant compartments over unique combinations of x, x' . Let us also assume that the fusion process is independent of the reactants' content. Therefore we have $h(\mathbf{n};x,x') = k w_{(x,x')}(\mathbf{n})$.

Since the propensity of this transition class is independent of the content of the two reactant compartments, the content functions are $f_c^0 = -1 \cdot k$ and $f_c^1 = 0 \cdot k$.

The moment equations for $\langle N \rangle$ and $\langle M^1 \rangle$ are therefore given by

$$\begin{aligned} \frac{d\langle N \rangle}{dt} &= \left\langle \sum_{\{x,x'\}} -1 \cdot k \cdot \frac{\mathbf{n}_x(\mathbf{n}_{x'} - \delta_{x,x'})}{(1 + \delta_{x,x'})} \right\rangle \\ &= \left\langle \sum_{x,x'} -1 \cdot k \cdot \frac{\mathbf{n}_x(\mathbf{n}_{x'} - \delta_{x,x'})}{2} \right\rangle \end{aligned} \quad (25)$$

$$\begin{aligned} &= \left\langle \sum_{x,x'} -\frac{k}{2} \cdot (\mathbf{n}_x \mathbf{n}_{x'} - \delta_{x,x'} \mathbf{n}_x) \right\rangle \\ &= -\frac{k}{2} \langle NN \rangle + \frac{k}{2} \langle N \rangle \end{aligned}$$

$$\frac{d\langle M^1 \rangle}{dt} = \left\langle \sum_{x,x'} 0 \cdot k \cdot \frac{\mathbf{n}_x(\mathbf{n}_{x'} - \delta_{x,x'})}{2} \right\rangle = 0. \quad (26)$$

Notice that in the first line of eq. (25) the sum is taken over unique combinations of x and x' (referred to as $\{x, x'\}$), while in the remaining lines of eq. (25) and in eq. (26) the sum is rewritten to go over all combinations of x and x' , which requires the state function to be corrected for double-counting.

Notice that eq. (25) for $\langle N \rangle$ depends on $\mathbf{n}_x \mathbf{n}_{x'}$, making the state function a second-degree polynomial. This causes $\langle N \rangle$ to depend on the moment $\langle (N)^2 \rangle = \langle NN \rangle$. An equation for $\langle NN \rangle$ can be derived using Itô's rule for counting processes (see A):

$$\begin{aligned} \frac{d\langle NN \rangle}{dt} &= \left\langle \sum_{x, x'} [(N-1)^2 - (N)^2] \cdot k \cdot \frac{\mathbf{n}_x (\mathbf{n}_{x'} - \delta_{x, x'})}{2} \right\rangle \\ &= \left\langle \sum_{x, x'} [-2N + 1] \cdot \frac{k}{2} \cdot (\mathbf{n}_x \mathbf{n}_{x'} - \delta_{x, x'} \mathbf{n}_x) \right\rangle \quad (27) \\ &= -k \langle NNN \rangle + \frac{3}{2} \langle NN \rangle - \frac{1}{2} \langle N \rangle. \end{aligned}$$

This demonstrates that in this scenario the equation for any $\langle (N)^k \rangle$ depends on $\langle (N)^{k+1} \rangle$, leading again to an infinite set of moment equations. Note however that this closure problem is different from the one of the previous scenario as it originates from *products* of moments (e.g. NNN), as opposed to higher order moments such as M^k . This illustrates that the compartmentalised systems considered here display two types of closure problems, which is an important difference to bulk chemical systems or compartmentalized systems in the large N limit.

We remark that for general polynomial content- and state functions, both closure problems can occur simultaneously, leading to products of multiple higher-order moments such as $\langle NM^3 \rangle$ or $\langle M^{2,0} M^{0,3} \rangle$, for instance.

Non-polynomial functions. In many practical cases, the involved rate functions may not be of polynomial form. This is the case, for instance, when considering enzyme kinetics inside compartments (e.g., Michaelis-Menten or Hill functions) or compartment fusion driven by non-polynomial coagulation kernels. In this case, the functions f_c^γ and/or w_{c, x_c} take more general, non-polynomial forms, causing the moment dynamics to depend on terms which cannot be expressed as moments at all. In order to study such systems using moment equations, suitable polynomial approximations are necessary.

2.4 A local polynomial (moment) approximation for compartmentalised reaction systems (LPAC)

The demonstration of the closure-related challenges outlined in section 2.3 also suggests a possible remedy. In case of polynomial content- and state functions f_c^γ and w_{c, x_c} , their degrees dictate the order of the moments and moment products appearing on the right-hand side of (9). Therefore, constraining the degree of f_c^γ and w_{c, x_c} will bound both the order of the moments and the degree of moment products. If we apply the

same constraints consistently to all the moments involved, this will ultimately lead to a closed system of moment equations.

To demonstrate this idea, consider maximum degrees δ_c and δ_s for the content- and state function, respectively. We can first derive equations for a given set of moments using eq. (8) and put them into their separated form. The resulting content- and state functions are then approximated by polynomials of degree δ_c and δ_s . Taking the expectations will lead to a linear combination of expected moments. These may involve additional expected moments, for which new equations have to be derived. The content- and state functions appearing on the right-hand side of these new equations are approximated again using polynomials of order δ_c and δ_s . This procedure is repeated until no new expected moments appear, resulting in a closed system of equations.

The simplest way to obtain polynomial approximations of the functions f_c^γ and w_{c, x_c} is to use truncated Taylor series around suitable expansion points \hat{x} and \hat{n} . To derive explicit expressions for the approximate moment equations, we first define the following shorthand notation

$$\mathcal{D}_{k,i}^\alpha := \frac{\partial^{\alpha_{k,i}}}{\partial (x_c)_{k,i}} \quad (28)$$

$$\xi_{k,i} := (x_c)_{k,i} - \hat{x}_i \quad (29)$$

$$\mathcal{D}_k^\beta := \frac{\partial^{\beta_k}}{\partial \mathbf{n}_{(x_c)_k}} \quad (30)$$

$$\boldsymbol{\eta}_k := \mathbf{n}_{(x_c)_k} - \hat{\mathbf{n}}_{(x_c)_k}, \quad (31)$$

where x_c is the set of reactant compartments of size r_c corresponding to the c -th transition class and $(x_c)_{k,i}$ denotes the i -th chemical species of the k -th compartment in x_c . The exponents $\alpha_{k,i}$ and β_k denote the differentiation orders associated with the content- and state functions, respectively.

The Taylor expansions of the content- and state functions can then be written as

$$\begin{aligned} f_c^\gamma(x_c) &= \sum_{\alpha_{1,1}=0}^{\infty} \dots \sum_{\alpha_{r_c,1}=0}^{\infty} \dots \sum_{\alpha_{1,d}=0}^{\infty} \dots \sum_{\alpha_{r_c,d}=0}^{\infty} \left[\right. \\ &\quad \left. (\mathcal{D}_{1,1}^\alpha \dots \mathcal{D}_{r_c,d}^\alpha) f_c^\gamma|_{(\hat{x}, \dots, \hat{x})} \right. \\ &\quad \left. \frac{(\xi_{1,1})^{\alpha_{1,1}} \dots (\xi_{r_c,d})^{\alpha_{r_c,d}}}{\alpha_{1,1}! \dots \alpha_{r_c,d}!} \right] \quad (32) \end{aligned}$$

$$= \sum_{\alpha} \mathcal{D}^\alpha f_c^\gamma|_{\hat{x}} \frac{\xi^\alpha}{\alpha!} \quad (33)$$

and

$$w_{c,x_c}(\mathbf{n}) = \sum_{\beta_1=0}^{\infty} \dots \sum_{\beta_{r_c}=0}^{\infty} \left[\begin{aligned} & (\mathcal{D}_1^{\beta_1} \dots \mathcal{D}_{r_c}^{\beta_{r_c}}) w_{c,x_c} |_{(\hat{\mathbf{n}}_{(x_c)_1}, \dots, \hat{\mathbf{n}}_{(x_c)_{r_c}})} \\ & \frac{(\eta_1)^{\beta_1} \dots (\eta_{r_c})^{\beta_{r_c}}}{\beta_1! \dots \beta_{r_c}!} \end{aligned} \right] \quad (34)$$

$$= \sum_{\beta} \mathcal{D}^{\beta} w_{c,x_c} |_{\hat{\mathbf{n}}} \frac{\eta^{\beta}}{\beta!}, \quad (35)$$

respectively.

If we substitute the expansions, eqs. (33) and (35), into the separated moment equation, eq. (9), we finally obtain the full explicit form of the Taylor-based moment approximation

$$\begin{aligned} \frac{d\langle M^{\gamma} \rangle}{dt} &= \sum_c \left\langle \sum_{x_c} f_c^{\gamma}(x_c) w_{c,x_c}(\mathbf{n}) \right\rangle \\ &\approx \sum_c \sum_{\alpha, \beta} \left\langle \sum_{x_c} \mathcal{D}^{\alpha} f_c^{\gamma} |_{\hat{x}} \mathcal{D}^{\beta} w_{c,x_c} |_{\hat{\mathbf{n}}} \frac{\xi^{\alpha} \eta^{\beta}}{\alpha! \beta!} \right\rangle. \end{aligned} \quad (36)$$

We now choose the first expansion point as $\hat{x} = (\hat{x}_i)_i$ such that its components are

$$\hat{x}_i = \frac{\langle M^{e_i} \rangle}{\langle N \rangle}, \quad (37)$$

where e_i is the i -th unit vector. This can be understood as an estimate of the mean compartment content. For the second expansion point we choose the expected number distribution

$$\hat{\mathbf{n}} = \langle \mathbf{n} \rangle. \quad (38)$$

This is particularly important as it allows us to conveniently translate the $\sum_x x^{\gamma} \eta$ terms arising in the Taylor expansion (36) into functions of moments as

$$\begin{aligned} \sum_x x^{\gamma} \eta &= \sum_x x^{\gamma} (\mathbf{n}_x - \langle \mathbf{n}_x \rangle) \\ &= \sum_x x^{\gamma} \mathbf{n}_x - \sum_x x^{\gamma} \langle \mathbf{n}_x \rangle \\ &= \sum_x x^{\gamma} \mathbf{n}_x - \left\langle \sum_x x^{\gamma} \mathbf{n}_x \right\rangle \\ &= M^{\gamma} - \langle M^{\gamma} \rangle. \end{aligned} \quad (39)$$

We can now plug the chosen expansion points into (36) to obtain the final compact form:

$$\begin{aligned} \frac{d\langle M^{\gamma} \rangle}{dt} &= \sum_c \sum_{\alpha} \sum_{\beta \leq e} \sum_{k=0}^{\alpha} \mathcal{D}^{\alpha} f_c^{\gamma} |_{\hat{x}} \mathcal{D}^{\beta} w_{c,x_c} |_{\langle \mathbf{n} \rangle} \binom{\alpha}{k} (-\hat{x})^k \\ &\quad \left\langle \left(M^{\alpha-k} - \langle M^{\alpha-k} \rangle \right)^{\beta} \right\rangle, \end{aligned} \quad (40)$$

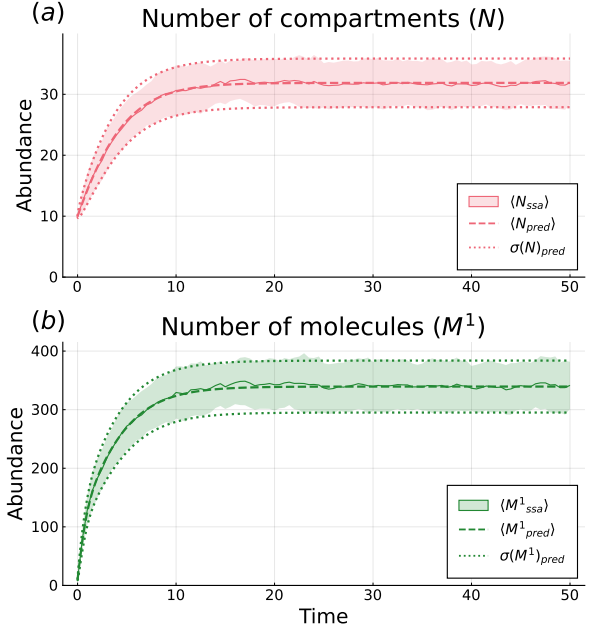


Figure 1: Comparison of the results obtained by averaging 100 trajectories of the stochastic simulation algorithm (SSA), shown by the solid line and shaded area, with the predictions of our moment-expansion method, shown by the dashed line and dotted boundaries. The solid and dashed lines denote average values, while the shaded and dot-bordered areas are the regions within one standard deviation. Panel (a) shows the statistics of the number of compartments (N) and panel (b) shows the statistics of the total number of molecules in the system (M^1).

where we used the standard multi-index notation for all operators involving tuples to arrive at the final compact form. See C for the precise definition of all multi-index operations used in our work. Note that eq. (40) relies on the assumption that the state function w_{c,x_c} is multilinear, as indicated by the summation domain $\beta \leq e$, i.e. $\beta_i \leq 1$ for all i . If we now truncate eq. (40) such that $|\alpha| \leq \delta_c$ and $|\beta| \leq \delta_s$ we obtain the final approximated moment equation for $\langle M^{\gamma} \rangle$.

3 Case studies

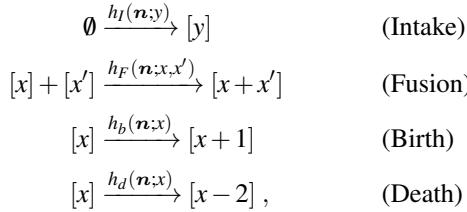
To test the proposed moment expansion method, we applied it to three different case studies. These examples are chosen to resemble characteristic features of biological systems such as non-linear propensities, interactions among compartments and feedback loops. We analyze the accuracy of our moment-approximation approach, by comparing it to exact Monte Carlo simulation. Moment equations were derived automatically by the *Compartmentor*[22] toolbox, which was extended to support the presented LPAC moment-expansion method. The resulting equations were solved using the *DifferentialEquations.jl*[25] package of the Julia programming language[26].

Case study	Statistic	Error
bBDF	N	6 %
	M^1	7 %
sAIC	N	30 %
	Z_1	34 %
	Q	30 %
MR	N	7 %
	$M^{1,0}$	49 %
	$M^{1,1}$	65 %

Table 1: Error quantifications in the three case studies: *Binary birth-death fusion* (bBDF), *Shared Antithetic Integral Controller* (sAIC) and *Mutual gene repression* (MR). Errors were calculated by taking the absolute distance between the moments estimated from Monte Carlo simulations and LPAC, dividing it by the Monte Carlo standard deviation and averaging the resulting value across all time points.

3.1 Binary birth-death-fusion process

We first tested our method on a simple system that features two nonlinear propensity functions. Compartments contain a single chemical species X which is synthesized with a constant rate k_b . For molecular turnover, we consider an annihilation reaction $2X \rightarrow \emptyset$ with rate constant k_d . Compartments enter the system at a rate k_I and their initial content is distributed according to an intake distribution π_I , which we consider to be a Poisson distribution with mean λ . Moreover, two compartments can fuse with each other with rate constant k_F . In total, the system is given by the transition classes



with propensity functions

$$h_I(\mathbf{n};y) = k_I \pi_I(y) \quad (41)$$

$$h_F(\mathbf{n};x,x') = k_F \frac{\mathbf{n}_x (\mathbf{n}_{x'} - \delta_{x,x'})}{1 + \delta_{x,x'}} \quad (42)$$

$$h_b(\mathbf{n};x) = k_b \mathbf{n}_x \quad (43)$$

$$h_d(\mathbf{n};x) = k_d \frac{x(x-1)}{2} \mathbf{n}_x, \quad (44)$$

where x, x' and y are variables representing the compartments' chemical content. Here we observe that both the fusion- and annihilation transitions involve propensities that are nonlinear in state and content, respectively.

Our goal is to use our moment-expansion method to study the mean and variance of the population moments N and M^1 . To this end, we require equations for the averages $\langle N \rangle$ and $\langle M^1 \rangle$ as well as the second-order moments $\langle N^2 \rangle$ and $\langle (M^1)^2 \rangle$

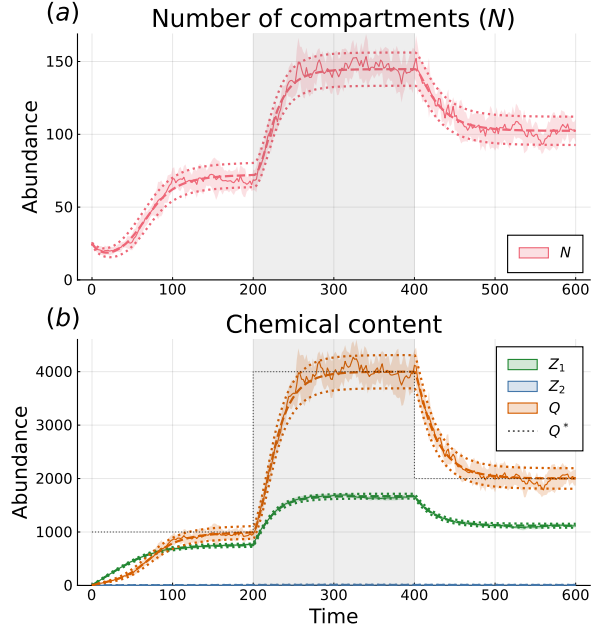


Figure 2: Comparison of the results obtained by averaging 8 SSA trajectories, shown by the solid line and shaded area, with the predictions of our moment-expansion method, shown by the dashed line and dotted boundaries. The solid and dashed lines denote average values, while the shaded and dot-bordered areas are the regions within one standard deviation. Panel (a) shows the statistics of the number of compartments (N) and panel (b) shows the statistics of the total number of molecules of different species in the system (Z_1 , Z_2 and Q), together with the controller's setpoint Q^* indicated by the grey dotted line.

from which variances can be obtained subsequently. However, deriving the equations for these moments leads to a closure problem due to the nonlinear propensities. We therefore employ a second-order polynomial approximation based on the Taylor series, which leads to a closed system of equations for the moments $\langle N \rangle$, $\langle N^2 \rangle$, $\langle M^1 \rangle$, $\langle (M^1)^2 \rangle$, $\langle M^2 \rangle$, $\langle (M^2)^2 \rangle$, $\langle NM^1 \rangle$, $\langle NM^2 \rangle$ and $\langle M^1 M^2 \rangle$. For further details refer to F.

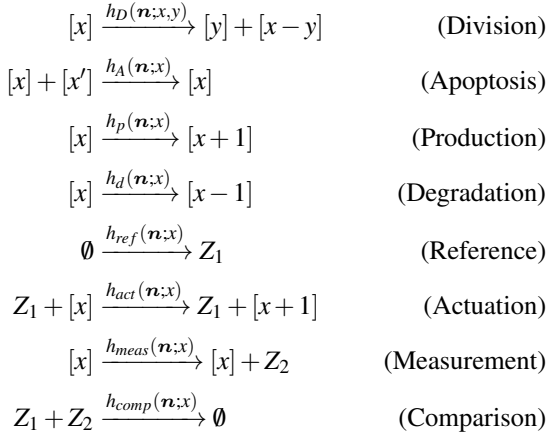
Figure 1 shows that the approximate statistics of N and M^1 (dashed and dotted lines) are in close agreement with Monte Carlo simulations (solid lines and shaded areas). Quantitative error measures are reported in table 1. On our installation, generating $n = 100$ Monte Carlo samples took 4.7s while solving the moment equations took $6.6 \cdot 10^{-4}$ s, corresponding to a speedup of about 7121 times.

3.2 Shared Antithetic Integral Controller

As a second case study we apply our approximation approach to a population-level feedback control motif that we analyzed previously [12]. This system is based on the *antithetic integral control* motif – a general biochemical control strategy that ensures robust perfect adaptation [27]. In contrast to the original scheme, the considered control system — termed *shared antithetic integral controller* (sAIC) — acts at the multicellular level and thereby provides a means to robustly regulate population-

level features such as the total amount of a produced species or the number of cells in the population. In our original work [12] we applied the sAIC to a simple cell population model and we adopt a similar model for the present case study.

Here we consider a population of cells undergoing division and apoptosis and within these cells a compartmentalised species Q is produced and degraded. This system is extended by the sAIC circuit by introducing two bulk controller species Z_1 , Z_2 and four additional transition classes. In total, the considered system is given by the following transition network



with propensity functions

$$h_D(\mathbf{n};x,y) = k_D \pi_D(y|x) x \mathbf{n}_x \quad (45)$$

$$h_A(\mathbf{n};x,x') = k_A \frac{\mathbf{n}_x(\mathbf{n}_{x'} - \delta_{x,x'})}{1 + \delta_{x,x'}} \quad (46)$$

$$h_p(\mathbf{n};x) = k_p \mathbf{n}_x \quad (47)$$

$$h_d(\mathbf{n};x) = k_d x \mathbf{n}_x \quad (48)$$

$$h_{ref}(\cdot) = k_{ref} \quad (49)$$

$$h_{act}(\mathbf{n}, Z_1; x) = k_{act} Z_1 \mathbf{n}_x \quad (50)$$

$$h_{meas}(\mathbf{n}; x) = k_{meas} x \mathbf{n}_x \quad (51)$$

$$h_{comp}(Z_1, Z_2) = k_{comp} Z_1 Z_2, \quad (52)$$

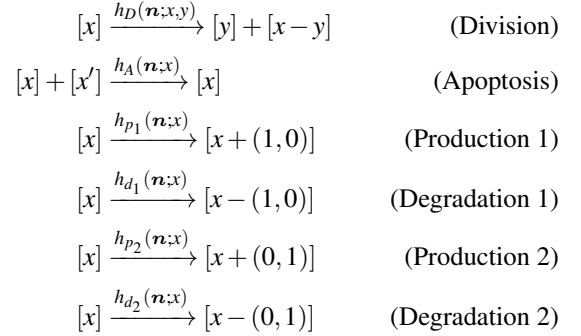
where x , x' and y are variables representing the compartments' chemical content, k_D , k_A , k_p , k_d , k_{ref} , k_{act} , k_{meas} and k_{comp} are the rate constants for the respective transition classes and π_D is the outcome distribution for cell division, where content is uniformly distributed among daughter cells. The *Division* and *Apoptosis* transition classes capture the dynamics of the cell population, where individual cells can divide and turn over. *Production* and *Degradation* describe the dynamics of the cell-internal species Q . Feedback-control is achieved via the four additional transition classes: *Reference* and *Actuation* are responsible for setting the target level of Q and promoting its production, while *Measurement* and *Comparison* provide a way to sense the current value of Q and downregulate its production. As we have shown previously, this circuit regulates the average total number of molecules $\langle Q \rangle$, i.e. $\langle M^1 \rangle$, to tunable set points $Q^* = k_{ref}/k_{meas}$, irrespective of all other system parameters.

For further details, the reader may refer to our original work [12] and G.

Figure 2 shows a controller with setpoints Q^* that change at time $t = 200$ and $t = 400$, and the total mass of the controlled species Q follows accordingly. Moreover, the statistics of the cell number and the total number of molecules are again approximated accurately by the moment-expansion method. Quantitative error estimates can be found in table 1.

3.3 Mutually repressing gene circuit in a cell population

In our last case study, we want to test our approach for a system that contains multiple chemical species that exhibit complex correlations. To this end, we take inspiration from developmental biology and consider a population of dividing cells that express two mutually repressing genes. Cell turnover is considered to be contact-dependent, where cells undergo apoptosis upon interacting with another cell from the population. The overall system is given by the transition classes



with propensity functions

$$h_D(\mathbf{n};x,y) = k_D \pi_D(y|x) \mathbf{n}_x \quad (53)$$

$$h_A(\mathbf{n};x,x') = k_A \frac{\mathbf{n}_x(\mathbf{n}_{x'} - \delta_{x,x'})}{1 + \delta_{x,x'}} \quad (54)$$

$$h_{p_1}(\mathbf{n};x) = k_p \frac{k_{R_1}}{k_{R_1} + x_2} \mathbf{n}_x \quad (55)$$

$$h_{d_1}(\mathbf{n};x) = k_d x_1 \mathbf{n}_x \quad (56)$$

$$h_{p_2}(\mathbf{n};x) = k_p \frac{k_{R_2}}{k_{R_2} + x_1} \mathbf{n}_x \quad (57)$$

$$h_{d_2}(\mathbf{n};x) = k_d x_2 \mathbf{n}_x, \quad (58)$$

where x , x' and y are variables representing the compartments' chemical content, k_D , k_A , k_p and k_d are the rate constants for the respective transition classes, k_{R_1} and k_{R_2} are Michaelis-Menten constants and π_D is the outcome distribution for cell division, where content is uniformly distributed among daughter cells.

Since the two internal species mutually repress each other (eq. (55) and (57)), we generally expect negative correlations between them. Here we want to study how the cell population dynamics impacts this correlation and to what extent our moment-approximation method is able to capture this. As a

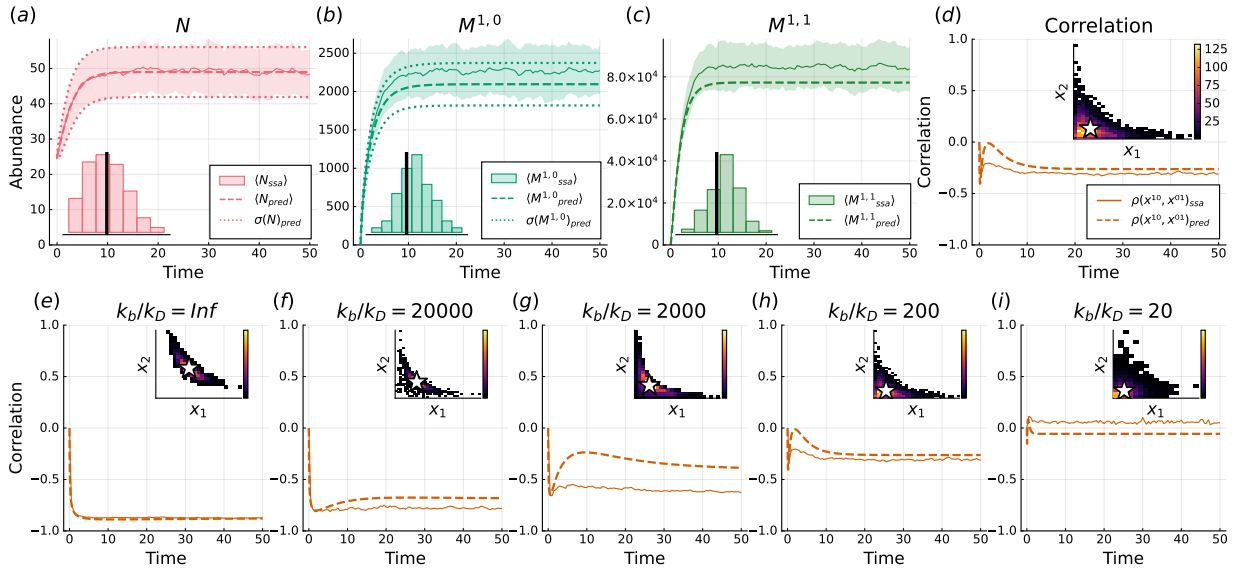


Figure 3: Comparison of the results obtained by averaging 128 SSA trajectories, shown by the solid line and shaded area, with the predictions of our moment-expansion method, shown by the dashed line and dotted boundaries. The solid and dashed lines denote average values, while the shaded and dot-bordered areas are the regions within one standard deviation. Panels (a-d) show the statistics of (a) the number of compartments N , (b) the total abundance of the first chemical species $M^{1,0}$, (c) the $M^{1,1}$ moment and (d) the Pearson correlation coefficient for the two chemical species. Insets of panels (a,b,c) respectively show the histograms of the N , $M^{1,0}$ and $M^{1,1}$ moments across the stochastic trajectories, with the black solid line indicating the predicted mean value. The inset of panel (d) shows the 2D histogram of the chemical content of compartments from all trajectories at the final timepoint of the SSA simulation, with the star symbol indicating the Taylor expansion point $(\langle M^{1,0} \rangle / \langle N \rangle, \langle M^{0,1} \rangle / \langle N \rangle)$. Panels (e-i) show the Pearson correlation and final-timepoint 2D histogram of the system in different k_b/k_D regimes: from (e) no cell turnover occurring with $k_b/k_D = \infty$, increasing the cell turnover speed (f-h) to the fastest (i) with $k_b/k_D = 20$.

measure for correlation, we use the Pearson correlation coefficient, which can be estimated from the approximate population moments as

$$\begin{aligned} \rho(x_1, x_2) &= \frac{\text{cov}(x_1, x_2)}{\sqrt{\text{var}(x_1)} \sqrt{\text{var}(x_2)}} \\ &\approx \frac{\langle M^{1,1} \rangle - \frac{\langle M^{1,0} \rangle \langle M^{0,1} \rangle}{\langle N \rangle}}{\sqrt{\langle M^{2,0} \rangle - \frac{\langle M^{1,0} \rangle^2}{\langle N \rangle}} \sqrt{\langle M^{0,2} \rangle - \frac{\langle M^{0,1} \rangle^2}{\langle N \rangle}}} \end{aligned} \quad (59)$$

(for details see E).

Figure 3, panels (a-d), shows the dynamics of the system in a regime where cell turnover and gene expression take place with a timescale ratio of $k_b/k_D = 200$, which is roughly the magnitude at which many physiological processes take place [28]. The respective quantitative error estimates can be found in table 1. Panels (e-i) show how the distribution of compartment content, together with their correlations, change over a spectrum of different timescale ratios. We speculate that the approximation (dashed lines) of moments $\langle M^{1,0} \rangle$, $\langle M^{1,1} \rangle$ and ρ (panels b-d) do not match the Monte Carlo estimation (solid lines) perfectly, likely because the distributions are more disperse than in the other case studies we presented in this work (see Appendix figs. 4 and 5). Thus, while the approximation is still able to capture the qualitative dynamics of the system, this case study also reveals the potential limitations of the approach

when dealing with strongly non-linear systems with disperse populations.

4 Discussion

Compartmentalization of biochemical reactions into compartments is a hallmark of biological systems. Studying the dynamic interplay between chemical reactions and compartmental dynamics is mathematically challenging, especially in the presence of noise. In this work we have developed LPAC, a systematic moment approximation to analyze the statistical properties of compartmentalized reaction systems. Our approach is based on our earlier work [10], but replaces *ad hoc* moment-closure approximations by polynomial approximations. This renders the approach applicable to a broader class of systems, including systems involving non-polynomial rate-laws. Our approach exploits the particular structure of the underlying moment equations, where individual terms can be written as expectations of products of two functions, one depending exclusively on the compartment content and one depending exclusively on the number distribution. We have further shown that these two functions give rise to two different types of closure problems, which is a key difference to bulk chemical systems as well as compartmentalized systems in the large N limit. The proposed moment-approximation technique addresses both of these closure problems and therefore always leads a closed system of moment equations. We have included this approach in a new

release of our previously developed moment generator *Compactor* [22], which can be used to derive moment equations in a fully automated manner for a broader class of systems.

To analyze the performance of our method, we have applied it to several models exhibiting nonlinear dynamics. We generally found that the approximate moments agreed very well with those obtained from exact Monte Carlo simulations. This is especially the case for the first two case studies, in which the compartment content was narrowly distributed (Figures 1, 2, 4 and 5). However, quantitative deviations were observed in situations where the distribution of molecular content is strongly disperse (Figures 3 and 6). This is in line with the fact that a simple truncated Taylor expansion was used as a polynomial approximation, which is guaranteed to be accurate only locally around the chosen expansion point. We remark, however, that our approach could in principle be extended to other polynomial approximations. Polynomial interpolation, for instance, could be used to achieve better approximation accuracy across larger domains, if a suitable set of interpolation nodes is chosen. This in turn could achieve accurate results even in the presence of strongly disperse or multimodal distributions. Also Bernstein polynomial may provide a promising approximation technique. As shown by Lunz *et al.* [11], they can be numerically better behaved than interpolants, although it is currently unclear how they perform on the particular class of systems that we considered in this work. Exploring these techniques more deeply in the context of these systems is an important goal for the future as it may expand the scope of our approach to an even larger class of systems.

5 Acknowledgements

We thank Jakob Ruess and Elisa Nerli for their helpful comments on the manuscript. The authors were supported by core funding of the Max Planck Institute of Molecular Cell Biology and Genetics and the BMBF under project number 031L0258C with the title “In-depth spatial organisation of hepatocellular carcinoma initiation”.

References

- [1] B. Alberts, A. Johnson, J. Lewis, M. C. Raff, K. Roberts, and P. Walter, “Molecular biology of the cell (fifth edition),” 2008.
- [2] D. Ramkrishna and M. R. Singh, “Population balance modeling: current status and future prospects,” *Annual review of chemical and biomolecular engineering*, vol. 5, pp. 123–146, 2014.
- [3] D. Ramkrishna, *Population balances: Theory and applications to particulate systems in engineering*. Elsevier, 2000.
- [4] L. Foret, J. E. Dawson, R. Villasenor, C. Collinet, A. Deutsch, L. Bruschi, M. Zerial, Y. Kalaidzidis, and F. Jülicher, “A general theoretical framework to infer endosomal network dynamics from quantitative image analysis,” *Current Biology*, vol. 22, no. 15, pp. 1381–1390, 2012.
- [5] M. A. Henson, “Dynamic modeling of microbial cell populations,” *Current opinion in biotechnology*, vol. 14, no. 5, pp. 460–467, 2003.
- [6] S. Waldherr, “Estimation methods for heterogeneous cell population models in systems biology,” *Journal of The Royal Society Interface*, vol. 15, no. 147, p. 20180530, 2018.
- [7] S. Rulands, F. Lescoart, S. Chabab, C. J. Hindley, N. Prior, M. K. Sznurkowska, M. Huch, A. Philpott, C. Blanpain, and B. D. Simons, “Universality of clone dynamics during tissue development,” *Nature physics*, vol. 14, no. 5, pp. 469–474, 2018.
- [8] D. Ramkrishna and J. Borwanker, “A puristic analysis of population balance-i,” *Chemical Engineering Science*, vol. 28, no. 7, pp. 1423–1435, 1973.
- [9] P. Thomas, “Intrinsic and extrinsic noise of gene expression in lineage trees,” *Scientific reports*, vol. 9, no. 1, p. 474, 2019.
- [10] L. Duso and C. Zechner, “Stochastic reaction networks in dynamic compartment populations,” *Proceedings of the National Academy of Sciences*, vol. 117, no. 37, pp. 22674–22683, 2020.
- [11] D. Lunz, J. F. Bonnans, and J. Ruess, “Revisiting moment-closure methods with heterogeneous multiscale population models,” *Mathematical Biosciences*, vol. 350, p. 108866, 2022.
- [12] L. Duso, T. Bianucci, and C. Zechner, “Shared antithetic integral control for dynamic cell populations,” in *2021 60th IEEE Conference on Decision and Control (CDC)*, pp. 2053–2058, IEEE, 2021.
- [13] V. Bansaye and S. Méléard, “Some stochastic models for structured populations: scaling limits and long time behavior,” *arXiv preprint arXiv:1506.04165*, 2015.
- [14] D. F. Anderson and A. S. Howells, “Stochastic reaction networks within interacting compartments,” *arXiv preprint arXiv:2303.14093*, 2023.
- [15] D. T. Gillespie, “Stochastic simulation of chemical kinetics,” *Annu. Rev. Phys. Chem.*, vol. 58, pp. 35–55, 2007.
- [16] C. Jia, A. Singh, and R. Grima, “Cell size distribution of lineage data: analytic results and parameter inference,” *Iscience*, vol. 24, no. 3, p. 102220, 2021.
- [17] P. Thomas and V. Shahrezaei, “Coordination of gene expression noise with cell size: analytical results for agent-based models of growing cell populations,” *Journal of the Royal Society Interface*, vol. 18, no. 178, p. 20210274, 2021.
- [18] C. Aditya, F. Bertaux, G. Batt, and J. Ruess, “Using single-cell models to predict the functionality of synthetic circuits at the population scale,” *Proceedings of the National Academy of Sciences*, vol. 119, no. 11, p. e2114438119, 2022.
- [19] D. Lunz, G. Batt, J. Ruess, and J. F. Bonnans, “Beyond the chemical master equation: stochastic chemical kinetics coupled with auxiliary processes,” *PLoS Computational Biology*, vol. 17, no. 7, p. e1009214, 2021.
- [20] B. Munsky and M. Khammash, “The finite state projection algorithm for the solution of the chemical master equation,” *The Journal of chemical physics*, vol. 124, no. 4, p. 044104, 2006.
- [21] D. Schnoerr, G. Sanguinetti, and R. Grima, “Approximation and inference methods for stochastic biochemical kinetics—a tutorial review,” *Journal of Physics A: Mathematical and Theoretical*, vol. 50, no. 9, p. 093001, 2017.
- [22] T. Pietzsch, L. Duso, and C. Zechner, “Compactor: a toolbox for the automatic generation of moment equations for dynamic compartment populations,” *Bioinformatics*, vol. 37, no. 17, pp. 2782–2784, 2021.
- [23] D. A. Dawson, B. Maisonneuve, J. Spencer, and D. Dawson, *Measure-valued Markov processes*. Springer, 1993.
- [24] V. Bansaye and S. Méléard, *Stochastic models for structured populations*, vol. 16. Springer, 2015.
- [25] C. Rackauckas and Q. Nie, “Differentials.jl—a performant and feature-rich ecosystem for solving differential equations in julia,” *Journal of Open Research Software*, vol. 5, no. 1, 2017.
- [26] J. Bezanson, A. Edelman, S. Karpinski, and V. B. Shah, “Julia: A fresh approach to numerical computing,” *SIAM Review*, vol. 59, no. 1, pp. 65–98, 2017.

- [27] C. Briat, A. Gupta, and M. Khammash, “Antithetic integral feedback ensures robust perfect adaptation in noisy biomolecular networks,” *Cell systems*, vol. 2, no. 1, pp. 15–26, 2016.
- [28] M. Shamir, Y. Bar-On, R. Phillips, and R. Milo, “Characteristic rates and timescales in cell biology,” *Cell*, vol. 164, pp. 1302–1302, 2016.
- [29] B. K. Øksendal and A. Sulem, *Applied stochastic control of jump diffusions*, vol. 498. Springer, 2007.

Supplementary Material

A Equations for products of moments

As mentioned in the main text, it is possible to derive moment equations for generic products of moments. Let us consider an m -ary product of moments

$$F(M^{\gamma_1}, \dots, M^{\gamma_m}) := M^{\gamma_1} \dots M^{\gamma_m}. \quad (\text{A.1})$$

Using Itô's rule for counting processes [29], it is straightforward to show that the expectation of this moment satisfies the differential equation

$$\begin{aligned} & \frac{d}{dt} \langle F(M^{\gamma_1}, \dots, M^{\gamma_m}) \rangle \\ &= \sum_c \left\langle \sum_{x_c} \left[F(M^{\gamma_1} + \Delta M_c^{\gamma_1}(x_c), \dots, M^{\gamma_m} + \Delta M_c^{\gamma_m}(x_c)) \right. \right. \\ & \quad \left. \left. - F(M^{\gamma_1}, \dots, M^{\gamma_m}) \right] g_c(x_c) w_{c,x_c}(\mathbf{n}) \right\rangle \\ &= \sum_c \left\langle \sum_{x_c} \left[(M^{\gamma_1} + \Delta M_c^{\gamma_1}(x_c)) \dots (M^{\gamma_m} + \Delta M_c^{\gamma_m}(x_c)) \right. \right. \\ & \quad \left. \left. - M^{\gamma_1} \dots M^{\gamma_m} \right] g_c(x_c) w_{c,x_c}(\mathbf{n}) \right\rangle. \end{aligned} \quad (\text{A.2})$$

$$(\text{A.3})$$

We can expand the products of all binomials in eq. (A.3) and get a sum of products of moments and $\Delta M_c^{\gamma_i}$ -terms. Each of these products contains, at most, $m-1$ moments.

Remark 1. Each term in the fully expanded version of eq. (A.3) has the form

$$\prod_{k \in \mathcal{H}} M^{\gamma_k} \underbrace{\prod_{h \in \mathcal{H}} \Delta M_c^{\gamma_h}(x_c) g_c(x_c) w_{c,x_c}(\mathbf{n})}_{f_c^{\mathcal{H}}(x_c)}, \quad (\text{A.4})$$

where if we define $\Gamma := \{\gamma_1, \dots, \gamma_m\}$, then $\mathcal{H} \subset \Gamma$ s.t. $|\mathcal{H}| \leq m-1$ and $\mathcal{H} = \Gamma \setminus \mathcal{H}$.

By substituting the definition of a population moment into eq. (A.4) we get that each term in eq. (A.3) can be written as follows:

$$\begin{aligned} & \left[\prod_{k \in \mathcal{H}} \sum_{i=1}^{|\mathcal{H}|} (x_{\mathcal{H}}^{(i)})^{\gamma_k} \mathbf{n}_{x_{\mathcal{H}}} \right] f_c^{\mathcal{H}}(x_c) w_{c,x_c}(\mathbf{n}) \\ &= \sum_{x_{\mathcal{H}}} g^{\mathcal{H}}(x_{\mathcal{H}}) w_{\mathcal{H}}(\mathbf{n}; x_{\mathcal{H}}) f_c^{\mathcal{H}}(x_c) w_{c,x_c}(\mathbf{n}) \\ &= \sum_{x_{\mathcal{H}}} f_c^{\mathcal{H}, \mathcal{H}}(x_c, x_{\mathcal{H}}) w_{c, \mathcal{H}}(\mathbf{n}; x_c, x_{\mathcal{H}}). \end{aligned} \quad (\text{A.5})$$

Here $x_{\mathcal{H}}$ is a tuple of compartment content symbols involved in the cross product identified by the set \mathcal{H} , in the same way as x_c represents the tuple of reactant compartments of a given transition c .

Now we can rewrite the whole moment equation for a generic product of moments as:

$$\begin{aligned} & \frac{d}{dt} \langle M^{\gamma_1} \dots M^{\gamma_m} \rangle \\ &= \sum_c \left\langle \sum_{x_c} \sum_{\mathcal{H}} \sum_{x_{\mathcal{H}}} f_c^{\mathcal{H}, \mathcal{H}}(x_c, x_{\mathcal{H}}) w_{c, \mathcal{H}}(\mathbf{n}; x_c, x_{\mathcal{H}}) \right\rangle \\ &= \sum_c \sum_{\mathcal{H}} \left\langle \sum_{(x_c, x_{\mathcal{H}})} f_c^{\mathcal{H}, \mathcal{H}}(x_c, x_{\mathcal{H}}) w_{c, \mathcal{H}}(\mathbf{n}; x_c, x_{\mathcal{H}}) \right\rangle. \end{aligned} \quad (\text{A.6})$$

This leads us directly to the following:

Lemma 1. Computing the contribution of a r_c -compartmental transition to the equation of a product of m moments is equivalent to a "virtual" transition involving $r_c + m - 1$ compartments, with a propensity that is still separable into a content-dependent function f and a state-dependent function w .

Remark 2. This means that all the results on approximating moment equations of the form

$$\frac{d \langle M^{\gamma} \rangle}{dt}$$

can also be applied to any arbitrary product of moments

$$\frac{d}{dt} \langle M^{\gamma_1} \dots M^{\gamma_m} \rangle$$

and therefore to derive the equation for the expectation of any arbitrary moment polynomial.

B Approximated moment equations

Let us now consider the separated form of a generic moment equation (9) and assume that all content and state functions have been approximated by suitable polynomials. Expanding the products leads to monomials of the form

$$C x_{c,1,1}^{\alpha_{c,1,1}} \dots x_{c,r_c,d}^{\alpha_{c,r_c,d}} \mathbf{n}_{x_{c,1}}^{\beta_{c,1}} \dots \mathbf{n}_{x_{c,r_c}}^{\beta_{c,r_c}}, \quad (\text{B.7})$$

where C contains all the constant terms of the expression.

Since the expectation and summation $\langle \sum_{x_c} \dots \rangle$ are linear, we can bring both of them in and around each monomial. With a rearrangement of the operands and then splitting the summation we get:

$$\begin{aligned} & \left\langle \sum_{x_c} C x_{c,1,1}^{\alpha_{c,1,1}} \dots x_{c,1,d}^{\alpha_{c,1,d}} \mathbf{n}_{x_{c,1}}^{\beta_{c,1}} \right. \\ & \quad \left. \dots x_{c,r_c,1}^{\alpha_{c,r_c,1}} \dots x_{c,r_c,d}^{\alpha_{c,r_c,d}} \mathbf{n}_{x_{c,r_c}}^{\beta_{c,r_c}} \right\rangle \\ &= C \left\langle \sum_{x_{c,1}} x_{c,1,1}^{\alpha_{c,1,1}} \dots x_{c,1,d}^{\alpha_{c,1,d}} \mathbf{n}_{x_{c,1}}^{\beta_{c,1}} \right. \\ & \quad \left. \dots \sum_{x_{c,r_c}} x_{c,r_c,1}^{\alpha_{c,r_c,1}} \dots x_{c,r_c,d}^{\alpha_{c,r_c,d}} \mathbf{n}_{x_{c,r_c}}^{\beta_{c,r_c}} \right\rangle \end{aligned} \quad (\text{B.8})$$

$$= C \left\langle M^{\alpha_{c,1}, \beta_{c,1}} \dots M^{\alpha_{c,r_c}, \beta_{c,r_c}} \right\rangle. \quad (\text{B.9})$$

Notation. Here we have used an extended notation for generalized population moments:

$$M^{\gamma,\sigma} := \sum_x x^\gamma n_x^\sigma. \quad (\text{B.10})$$

With the term order we still refer to $|\gamma|$, while we refer to $|\sigma|$ as n -order.

Remark 3. If the compartment events follow mass-action-like kinetics, then their state function w is multilinear; i.e. it is linear with respect to each single reactant compartment symbol. This means that it can only generate moments that have a maximum n -order of 1 each.

Lemma 2. If the polynomial approximating the content function f has degree δ , then for any moment $M^{\gamma,\sigma}$ that appears in the approximated moment equation it holds $|\gamma| \leq \delta$.

Proof. Since the degree of the polynomial is δ , then by definition the sum of the α exponents of all monomials in eq. (B.7) is bounded by δ . This means that the order of all moments generated by these monomials is also necessarily bounded by δ . \square

Remark 4. From the proof we also get a stronger result: the total order of the moments in any moment product is also bounded by the approximation degree δ .

Lemma 3. If the polynomial approximating the content function w has degree ε , then the total n -order of any moment product

$$\langle M^{\gamma_1,\sigma_1} \dots M^{\gamma_m,\sigma_m} \rangle \quad (\text{B.11})$$

is bounded by ε , that is $\sum_{i=1}^m |\sigma_i| \leq \varepsilon$.

Proof. Since the degree of the polynomial approximating w is ε , then all monomials in eq. (B.7) have a total order of the β exponents that is bounded by ε . Following the derivation of eq. (B.8) we then obtain that any product of moments obtained by the approximation and truncation procedure has a total n -order bounded by ε . \square

Remark 5. This also means that the number of moments involved in any product appearing on the right-hand side is also bounded. In case the compartment events follow a mass-action-like kinetics, then the number of moments must be $\leq \varepsilon$.

The above results lead to the following:

Theorem 1. Given an equation for any arbitrary moment or product of moments and two approximation degrees $\delta, \varepsilon \in \mathbb{N}$, the approximation of order (δ, ε) of such equation can be solved through a system of moment equations with the same approximation order and the system is closed.

Proof. Using lemmas 2 and 3 we obtain that the equation for any desired moment, approximated at order (δ, ε) only contains products of moments of total order δ and total n -order

ε . Furthermore any product of moments additionally required in the system of equations can also be described with an approximated equation only containing products of moments of total order δ and total n -order ε . Since order and n -order are positive integers and bounded by δ and ε respectively, then the combinations of moments that can appear in a product of moments are finite and this proves that the system of equations is closed. \square

We therefore have a simple algorithm allowing to always derive a closed set of moment equations: first derive the equations for all the moments of interest, substituting all content and state functions with suitable polynomials of limited degree; then collect all moments and moment products these equations depend on and iteratively apply the same procedure for all those we still have no equation for. This procedure will terminate and produce a closed set of moment equations.

C Multi-index notation and operators

Throughout this work, we rely on standard multi-index notation to make the equations more compact and easier to read. Multi-index notation allows common operators that accept integer indices as arguments to be extended to ordered tuples of indices. Here we provide the definitions of multi-index operators used in our work.

A d -dimensional multi-index is defined as a d -tuple:

$$\alpha = (\alpha_1, \alpha_2, \dots, \alpha_d) \in \mathbb{N}_0^d.$$

If $\alpha, \beta \in \mathbb{N}_0^d$ and $x \in \mathbb{R}^d$ we can define:

Sum

$$\alpha + \beta = (\alpha_1 + \beta_1, \dots, \alpha_d + \beta_d)$$

Partial ordering

$$\alpha \leq \beta = (\alpha_1 \leq \beta_1, \dots, \alpha_d \leq \beta_d)$$

Power

$$x^\alpha = x_1^{\alpha_1} \dots x_d^{\alpha_d}$$

Factorial

$$\alpha! = \alpha_1! \dots \alpha_d!$$

Binomial coefficient

$$\binom{\alpha}{\beta} = \binom{\alpha_1}{\beta_1} \dots \binom{\alpha_d}{\beta_d}$$

Partial derivatives

$$\mathcal{D}^\alpha = \frac{\partial^{\alpha_1}}{\partial x_1^{\alpha_1}} \dots \frac{\partial^{\alpha_d}}{\partial x_d^{\alpha_d}}$$

D Including bulk chemical species and reactions

It is possible to have systems where a compartment population, with its internal chemistry, interacts with chemistry occurring in the bulk of the outer medium. We gave an example coming from bio-engineering in section 3.2, but many other biological systems have this characteristic too.

Here we want to show how the same mathematical framework that we used can be extended in order to account for bulk chemical species and how their chemistry can be coupled to the compartmentalised system and its transitions.

Let us recall the generic 3-term form of a moment equation, from eq. (8):

$$\frac{d\langle M^\gamma \rangle}{dt} = \sum_c \left\langle \sum_{x_c} \Delta M_c^\gamma(x_c) g_c(x_c) w_{c,x_c}(\mathbf{n}) \right\rangle.$$

We introduce a new stochastic state vector \mathbf{B} , which collects the copy numbers of all bulk chemical species. We can now account for the bulk chemical state in the moment equations by assuming the transition propensities also have a dependence on the bulk state:

$$\frac{d\langle M^\gamma \rangle}{dt} = \sum_c \left\langle \sum_{x_c} \Delta M_c^\gamma(x_c) g_c(x_c) w_{c,x_c}(\mathbf{n}) b_c(\mathbf{B}) \right\rangle. \quad (\text{D.12})$$

Where the *bulk-dependent* rate function b_c would have a constant value of 1 in each transition class that does not depend on the bulk chemical state.

Analogously to the presented moment equations, we can also derive differential equations for the evolution of the expected bulk state:

$$\frac{d\langle \mathbf{B} \rangle}{dt} = \sum_c \left\langle \sum_{x_c} \Delta B_c(x_c) g_c(x_c) w_{c,x_c}(\mathbf{n}) b_c(\mathbf{B}) \right\rangle. \quad (\text{D.13})$$

Chemical reactions that occur in the bulk, without involving compartments and their content, are represented by transition classes that do not involve any reactant compartment, i.e. with $x_c = \{\}$. In this case the corresponding terms in eq. (D.13) contain a ΔB_c that is independent of x_c such that the inner sum simplifies to $\Delta B_c \langle b_c(\mathbf{B}) \rangle$. In the special case where there are no chemical interactions between any bulk and compartmentalised chemical species, eq. (D.13) would further simplify to a conventional moment equation for bulk chemical systems

$$\frac{d\langle \mathbf{B} \rangle}{dt} = \sum_c \Delta B_c \langle b_c(\mathbf{B}) \rangle. \quad (\text{D.14})$$

The function of the bulk state $b_c(\mathbf{B})$ can then be polynomially expanded around the mean state $\langle \mathbf{B} \rangle$ in the same way as the state function $w_{c,x_c}(\mathbf{n})$, obtaining a closed set of moment equations that account for bulk quantities and moment-bulk cross products.

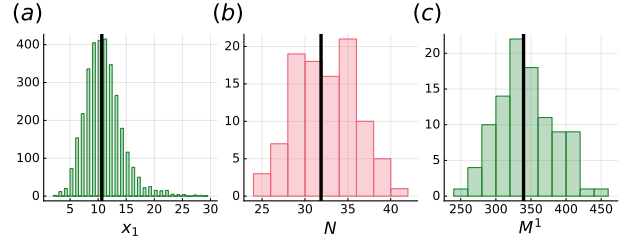


Figure 4: Histograms for the distributions of (a) the cellular content variable x_1 , (b) the number of cells in the system N and (c) the total mass of x_1 in the system M^1 in the *Binary birth-death-fusion* case study. The solid black lines in each panel shows the estimated values of $\langle M^1 \rangle / \langle N \rangle$, $\langle N \rangle$ and $\langle M^1 \rangle$, respectively, as computed by the approximation.

E Pearson correlation coefficient in compartment populations

We use a mean-field approximation of the Pearson correlation coefficient in order to be able to compute it from the population moments that are already available in the *Mutual Repression* case study from section 3.3.

We use the following base approximations:

$$\begin{aligned} \text{cov}(x_1, x_2) &= \left\langle \frac{M^{1,1}}{N} \right\rangle - \left\langle \frac{M^{1,0}}{N} \right\rangle \left\langle \frac{M^{0,1}}{N} \right\rangle \\ &\approx \frac{\langle M^{1,1} \rangle}{\langle N \rangle} - \frac{\langle M^{1,0} \rangle \langle M^{0,1} \rangle}{\langle N \rangle^2} \end{aligned} \quad (\text{E.15})$$

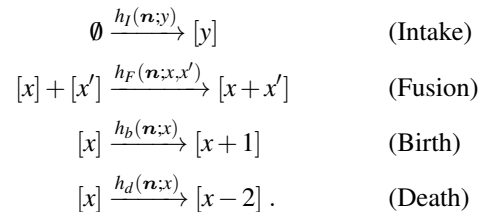
$$\begin{aligned} \text{var}(x_1) &= \left\langle \frac{M^{2,0}}{N} \right\rangle - \left\langle \frac{M^{1,0}}{N} \right\rangle^2 \\ &\approx \frac{\langle M^{2,0} \rangle}{\langle N \rangle} - \frac{\langle M^{1,0} \rangle^2}{\langle N \rangle^2}. \end{aligned} \quad (\text{E.16})$$

Plugging them into the Pearson correlation's definition we get the formula that we use in the analysis of the case study:

$$\begin{aligned} \rho(x_1, x_2) &= \frac{\text{cov}(x_1, x_2)}{\sqrt{\text{var}(x_1)} \sqrt{\text{var}(x_2)}} \\ &\approx \frac{\langle M^{1,1} \rangle - \frac{\langle M^{1,0} \rangle \langle M^{0,1} \rangle}{\langle N \rangle}}{\sqrt{\langle M^{2,0} \rangle - \frac{\langle M^{1,0} \rangle^2}{\langle N \rangle}} \sqrt{\langle M^{0,2} \rangle - \frac{\langle M^{0,1} \rangle^2}{\langle N \rangle}}}. \end{aligned} \quad (\text{E.17})$$

F Case study: Binary birth-death-fusion process

As detailed in section 3.1 of the main text, the system is defined by the transition classes



with propensity functions

$$h_I(\mathbf{n}; y) = k_I \pi_I(y) \quad (\text{F.18})$$

$$h_F(\mathbf{n}; x, x') = k_F \frac{\mathbf{n}_x (\mathbf{n}_{x'} - \delta_{x,x'})}{1 + \delta_{x,x'}} \quad (\text{F.19})$$

$$h_b(\mathbf{n}; x) = k_b \mathbf{n}_x \quad (\text{F.20})$$

$$h_d(\mathbf{n}; x) = k_d \frac{x(x-1)}{2} \mathbf{n}_x. \quad (\text{F.21})$$

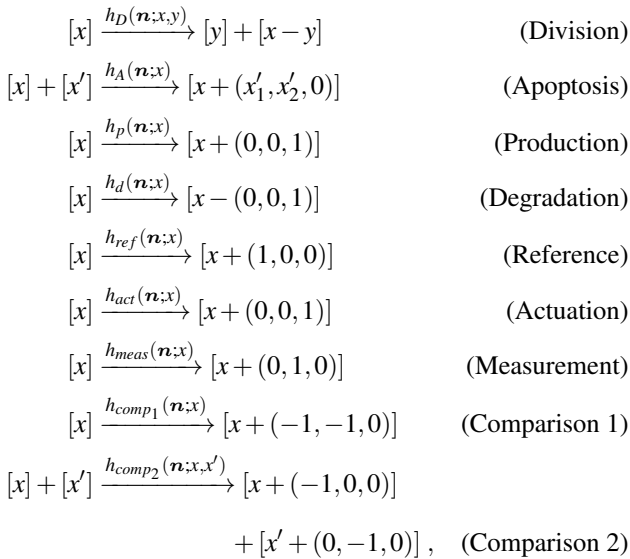
The complete set of moment equations for this case study, together with the code to generate them automatically with *Compator*, can be found in the corresponding Jupyter notebook in the *Compator* repository on GitHub.

G Case study: Shared Antithetic Integral Controller

The *sAIC* case study features a bulk chemistry that is coupled to the compartmentalised system. As detailed in Supplementary Material appendix D, bulk chemistry can be integrated into the mathematical framework with little symbolic overhead. *Compator*, our tool for generating the moment equations, does however not yet support this extension. We have therefore resorted to “virtualising” the *sAIC* bulk chemistry into a set of compartmentalised transitions that have identical dynamics.

The internal compartment state is given by the 3-species tuple (Z_1, Z_2, Q) , where Z_1 and Z_2 are the two bulk controller chemical species and Q is the actual internal measured species. Species Z_1 and Z_2 are therefore virtually spread among the compartments in the system and their total amounts are given by the moments $M^{1,0,0}$ and $M^{0,1,0}$ respectively. The transition classes are modified in order to conserve Z_1 and Z_2 in case of compartmental events. Furthermore, the *Comparison* reaction is split into two transitions, in order to account for the reactant molecules to virtually belong either to the same compartment or to two different ones.

The full augmented transition network is represented by the following diagram:



while the propensity functions are as follows:

$$h_D(\mathbf{n}; x, y) = k_D \pi_D(y | x) x_3 \mathbf{n}_x \quad (\text{G.22})$$

$$h_A(\mathbf{n}; x, x') = k_A \frac{\mathbf{n}_x (\mathbf{n}_{x'} - \delta_{x,x'})}{1 + \delta_{x,x'}} \quad (\text{G.23})$$

$$h_p(\mathbf{n}; x) = k_p \mathbf{n}_x \quad (\text{G.24})$$

$$h_d(\mathbf{n}; x) = k_d x_3 \mathbf{n}_x \quad (\text{G.25})$$

$$h_{ref}(\mathbf{n}; x) = \frac{k_{ref}}{N} \mathbf{n}_x \quad (\text{G.26})$$

$$h_{act}(\mathbf{n}; x) = k_{act} M^{1,0,0} \mathbf{n}_x \quad (\text{G.27})$$

$$h_{meas}(\mathbf{n}; x) = k_{meas} x_3 \mathbf{n}_x \quad (\text{G.28})$$

$$h_{comp1}(\mathbf{n}; x) = k_{comp1} x_1 x_2 \mathbf{n}_x \quad (\text{G.29})$$

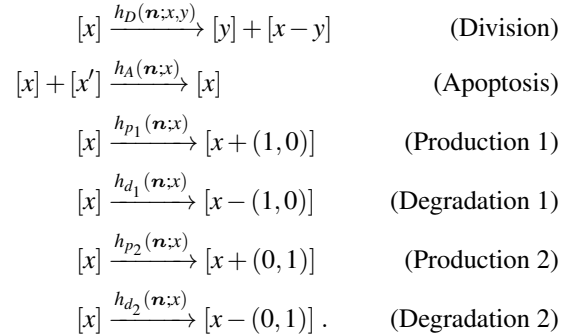
$$h_{comp2}(\mathbf{n}; x, x') = k_{comp2} x_1 x'_2 \frac{\mathbf{n}_x (\mathbf{n}_{x'} - \delta_{x,x'})}{1 + \delta_{x,x'}}. \quad (\text{G.30})$$

The complete set of moment equations for this case study, together with the code to generate them automatically with *Compator*, can be found in the corresponding Jupyter notebook in the *Compator* repository on GitHub.

H Case study: Mutually repressing gene circuit in a cell population

This case study features two internal chemical species, representing levels of gene expression, each inhibiting the production of the other through a repressor Michaelis-Menten type of kinetics. This internal dynamics is then imposed on a population of dividing cells, which size is kept in check by a binary cell death, i.e. a bi-compartmental transition in which one of the reactant compartments leaves the population.

The full transition network is represented by the following diagram:



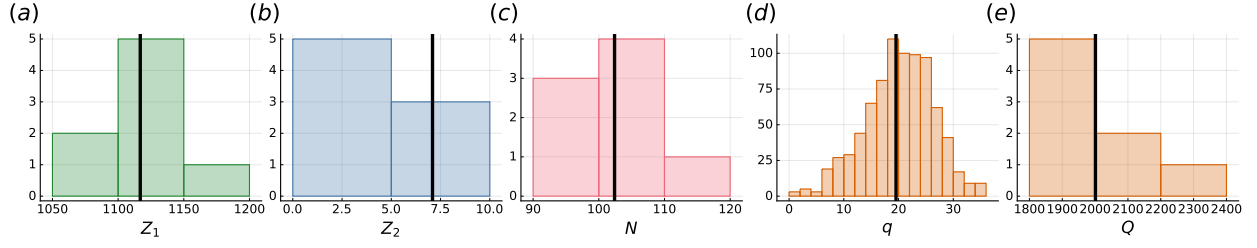


Figure 5: Histograms for the distributions of (a,b) the bulk controller species Z_1 and Z_2 respectively, (c) the number of cells in the system N , (d) the cellular content variable q and (e) the total mass of q in the system $Q = M^1$ in the *Shared Antithetic Integral Controller* case study. The solid black lines in each panel shows the estimated values of $\langle Z_1 \rangle$, $\langle Z_2 \rangle$, $\langle N \rangle$, $\langle Q \rangle / \langle N \rangle$ and $\langle Q \rangle$, respectively, as computed by the approximation.

While the propensity functions are as follows:

$$h_D(\mathbf{n}; x, y) = k_D \pi_D(y | x) \mathbf{n}_x \quad (\text{H.31})$$

$$h_A(\mathbf{n}; x, x') = k_A \frac{\mathbf{n}_x (\mathbf{n}_{x'} - \delta_{x,x'})}{1 + \delta_{x,x'}} \quad (\text{H.32})$$

$$h_{p_1}(\mathbf{n}; x) = k_p \frac{k_{R_1}}{k_{R_1} + x_2} \mathbf{n}_x \quad (\text{H.33})$$

$$h_{d_1}(\mathbf{n}; x) = k_d x_1 \mathbf{n}_x \quad (\text{H.34})$$

$$h_{p_2}(\mathbf{n}; x) = k_p \frac{k_{R_2}}{k_{R_2} + x_1} \mathbf{n}_x \quad (\text{H.35})$$

$$h_{d_2}(\mathbf{n}; x) = k_d x_2 \mathbf{n}_x. \quad (\text{H.36})$$

The complete set of moment equations for this case study, together with the code to generate them automatically with Compator, can be found in the corresponding Jupyter notebook in the Compator repository on GitHub.

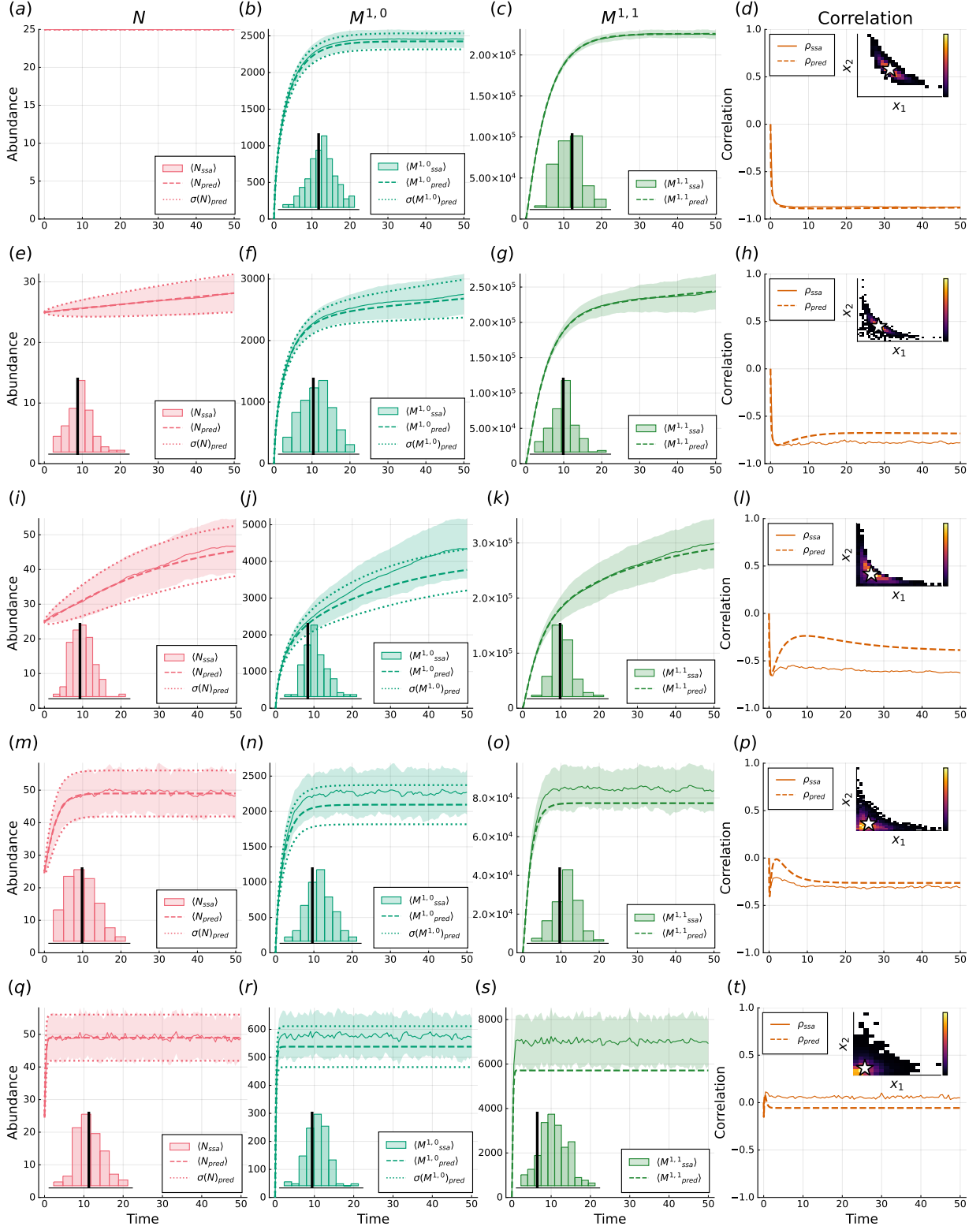


Figure 6: Comparison of the results obtained by averaging 128 SSA trajectories, shown by the solid line and shaded area, with the predictions of our moment-expansion method, shown by the dashed line and dotted boundaries. The solid and dashed lines denote average values, while the shaded and dot-bordered areas are the regions within one standard deviation. The layout of the panels for each row follows that of (fig. 3, a-d), while the rows correspond to the different k_b/k_D regimes as in (fig. 3, e-i): (a-d) $k_b/k_D = \infty$, (e-h) $k_b/k_D = 20000$, (i-l) $k_b/k_D = 2000$, (m-p) $k_b/k_D = 200$, (q-t) $k_b/k_D = 20$.